https://doi.org/10.5194/tc-2019-261
Preprint. Discussion started: 9 December 2019

The Cryosphere Discussions

A linear model to derive melt pond depth from hyperspectral data

Marcel König[1], Natascha Oppelt[1]

[1]Department of Geography, Kiel University, Kiel, 24118, Germany

Correspondence to: Marcel König (koenig@geographie.uni-kiel.de)

Abstract. Melt ponds are key elements in the energy balance of Arctic sea ice. Observing their temporal evolution is crucial for understanding melt processes and predicting sea ice evolution. Remote sensing is the only technique that enables large-scale observations of Arctic sea ice. However, monitoring vertical melt pond evolution in this way is challenging because most of the optical signal reflected by a pond is defined by the scattering characteristics of the underlying ice. Without knowing the influence of melt water on the reflected signal, the water depth cannot be determined. To solve the problem, we simulated the way melt water changes the reflected spectra of bare ice. We developed a model based on the slope of the log-scaled remote sensing reflectance at 710 nm. We validated the model using 49 in situ melt pond spectra and corresponding depths from ponds on dark and bright ice. Retrieved pond depths are precise ($RMSE$ = 2.81 cm) and highly correlated with in situ measurements (r = 0.89; p = 4.34e-17). The model further explains a large portion of the variation in pond depth (R^2 = 0.74). Our results indicate that pond depth is retrievable from optical data under clear sky conditions. This technique is potentially transferrable to hyperspectral remote sensors on UAVs, aircraft and satellites.

1 Introduction

Melt ponds on sea ice are key elements for the Arctic energy budget. They are a main driver of the ice-albedo-feedback mechanism (Curry et al., 1995). Pond evolution can be linked to observations of ocean and atmosphere, for validation of ice and climate models and future sea ice prediction, e.g. Schröder et al. (2014) show that spring melt pond fraction can be used to forecast September sea ice area.

Synoptic observations of melt pond evolution are only possible with satellite remote sensing. Optical sensors with an adequate spatial resolution that operate in the visible and near infrared (NIR) wavelength region enable a monitoring of pond water characteristics.

The reflected optical signal from open melt ponds contains information on the pond water, the pond bottom, i.e. underlying ice, and skylight reflected at the water surface. The color of melt ponds ranges from bright blue to almost black and is primarily defined by the scattering and to a lesser degree by the absorption characteristics of the pond bottom (Lu et al., 2016, 2017). Different radiative transfer models for melt ponds on sea ice exist (e.g. Lu et al., 2017; Malinka et al., 2018) but their capability to derive pond depth varies. To our knowledge, the most accurate model is the one presented in Malinka et al. (2018) resulting in an R^2 of 0.62 ($N = 26$) for pond depths between 6 cm and 50 cm under and different illumination conditions. Their model

https://doi.org/10.5194/tc-2019-261
Preprint. Discussion started: 9 December 2019

links pond albedo at various sky conditions to pond depth and transport scattering coefficient and thickness of the bottom ice. Inverse computations accurately reproduced in situ albedo spectra (relative root mean square difference ($rRMSD$) < 1.5%) but pond depth retrieval was more uncertain ($rRMSD$ = 65%). Therefore, our motivation is to 1) improve the limited accuracy of existing models and 2) develop an easy-to-use approach for deriving melt pond depth using hyperspectral data.

We hypothesize that instead of using the entire spectrum, selecting bands at certain wavelengths improves the retrieval of pond depth from optical data. The penetration depth of light into water is highest in the blue region of the electromagnetic spectrum and decreases with increasing wavelength. This means that with increasing wavelength the influence of the water column's attenuation on the optical signal increases (Pope and Fry, 1997). Morassutti and Ledrew (1996) stated that the influence of water absorption on the pond albedo increases towards the infrared wavelength region and Lu et al. (2016) found that pond albedo significantly depends on pond depth in the wavelength region between 600 nm and 900 nm. In this paper, we present a simple model, based on the absorption of near infrared light in water to retrieve pond depth from hyperspectral optical measurements under clear sky conditions.

2 Methods

We use spectral data of bare ice surfaces to simulate melt pond spectra for model development, and validate the model with in situ melt pond measurements acquired during RV *Polarstern* cruise PS106 in summer 2017.

2.1 Observational data

We used two instrument setups for acquisition of optical data. For most measurements, we used a combination of two Ocean Optics STS-VIS spectrometers (Ocean Optics Inc., USA). One spectrometer pointing downwards and equipped with a 1° fore optic; the other pointing upwards and equipped with a cosine collector. Both instruments cover the wavelength region from ~ 340 nm to ~ 820 nm with a spectral sampling rate < 1 nm and an spectral resolution of 3.0 nm (Ocean Optics, 2019). We used a Labsphere Spectralon 99 % diffuse reflectance standard (Labsphere Inc., USA) as white reference and applied the data from the second spectrometer to correct the reflectance spectra for changes in downwelling irradiance. For each measurement, we computed the average of 30 single spectra. Both instruments were mounted to the end of a pole to avoid influences of the polar clothes on the measurements. We also attached a camera to the setup to take photographs of each measurement site (Figure 1).

Some of the data used in this study was acquired within the scope of a goniometer experiment. For these measurements, we used an Ibsen Freedom VIS FSV-305 spectrometer (Ibsen Photonics A/S, Denmark) with a spectral sampling rate < 1 nm and a spectral resolution of 1.8 nm covering the wavelength range from ~ 360 nm to ~ 830 nm (Ibsen Photonics, 2019). The spectrometer has been equipped with an optical fiber and a 1° fore optic that were attached to a field goniometer (Figure 2). We used the above-mentioned Spectralon panel as white reference after each azimuthal scan and computed an average reflectance from 20 spectra.

The quantity measured with both spectrometer setups is the remote sensing reflectance $[sr^{-1}]$ (R_{rs}) above the water surface:

https://doi.org/10.5194/tc-2019-261
Preprint. Discussion started: 9 December 2019

$$R_{rs} = \frac{L_u}{E_d}, \quad (1)$$

where L_u is upwelling radiance $[W/(m^2\ nm\ sr)]$ measured by the downwards-pointing sensor and E_d is downwelling irradiance $[W/(m^2\ nm)]$ derived from the Spectralon measurement as

$$E_d = \frac{L_S \cdot \pi}{R_S}, \quad (2)$$

where R_S is the isotropic reflectance of the Spectralon panel, and L_S is a radiance measurement $[W/(m^2\ nm\ sr)]$ of the Spectralon panel.

2.1.1 Ice spectra

On 15 June 2017, we collected spectra from three bright and one dark bare ice surface with the Ocean Optics (Gege et al., 2019) setup under stable diffuse illumination conditions indicated by the negligible standard deviation (Figure 1).

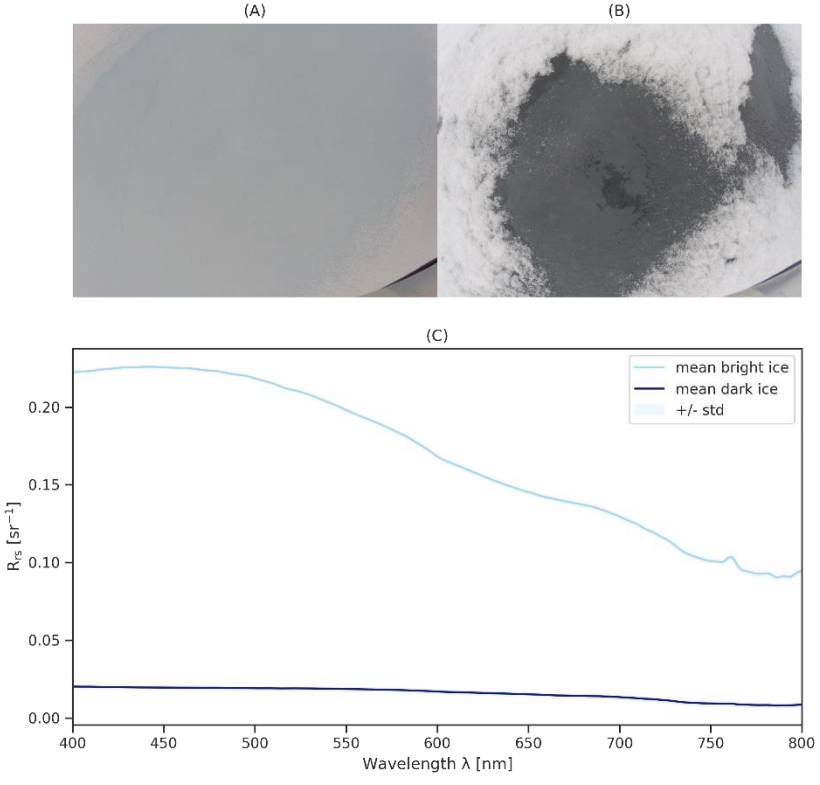

Figure 1: Photos of bright (A) and dark (B) bare ice surfaces and respective reflectance spectra (C).

https://doi.org/10.5194/tc-2019-261
Preprint. Discussion started: 9 December 2019

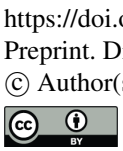

The Cryosphere Discussions
Open Access
EGU

On 2 July 2017 between 22:28 UTC and 23:11 UTC, we performed twelve nadir measurements of a bare ice surface under clear sky conditions and a mean sun zenith angle of 74.89° with the Ibsen setup (Gege and König, 2019). Here, we use the average spectrum (Figure 2). The large standard deviation may be attributed to surface metamorphism during the measurement.

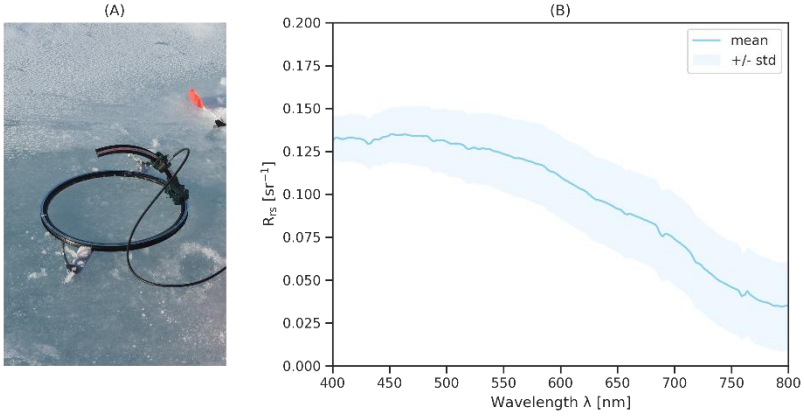

Figure 2: Ibsen bare ice measurement setup (A). Spectra used in this study (B) were taken at nadir.

2.1.2 Pond measurements

On 10 June 2017, we collected 49 melt pond spectra (Gege et al., 2019) and corresponding pond depths in three melt ponds. Two of the ponds had a bright blue color while the third one was very dark, which is also apparent in Figure 3.

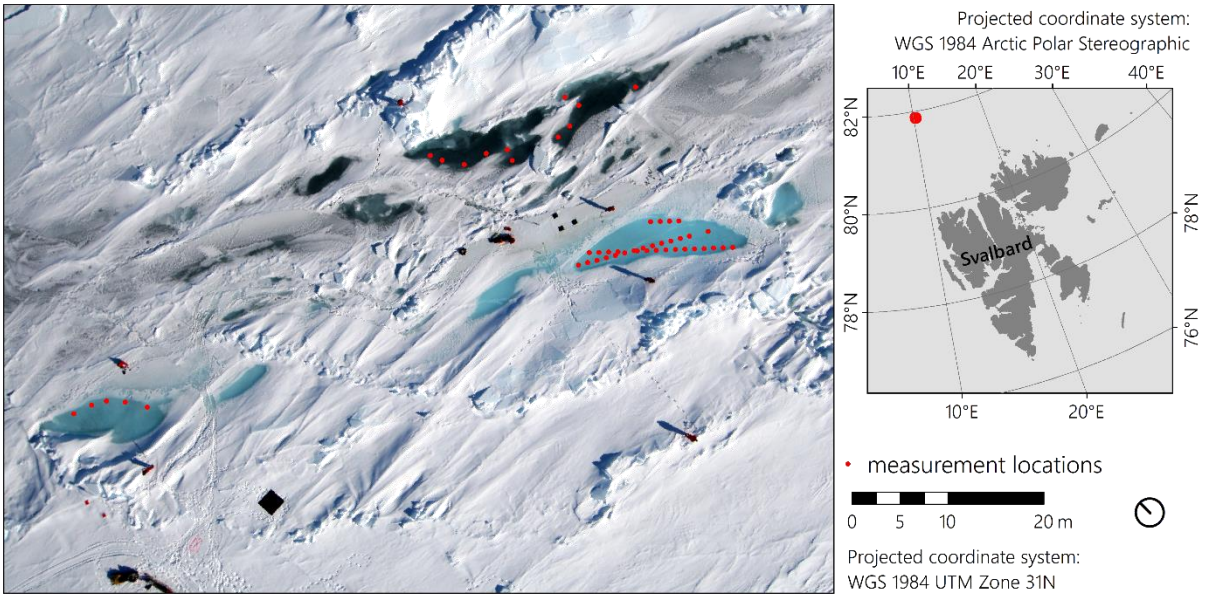

Figure 3: Overview of measurement sites in the three ponds. Aerial photo: Gerit Birnbaum.

At each pond, we referenced the Ocean Optics spectrometers using the Spectralon panel before data acquisition. We performed spectral measurements from the edge of the pond or waded through the pond avoiding shading. We did not observe any wind

https://doi.org/10.5194/tc-2019-261
Preprint. Discussion started: 9 December 2019

induced disturbances of the water surface and waited for the water surface to settle before performing measurements inside the ponds. All measurements were performed under clear sky conditions between 11:45 UTC and 14:05 UTC, and corresponding sun zenith angles between 58.90° and 61.04°. Directly after each spectral measurement, we used a folding ruler to measure pond depth at the same location. Depths ranged between 6 cm and 25 cm with an average of 17.60 cm. Figure 4 illustrates the melt pond spectra and corresponding pond depths.

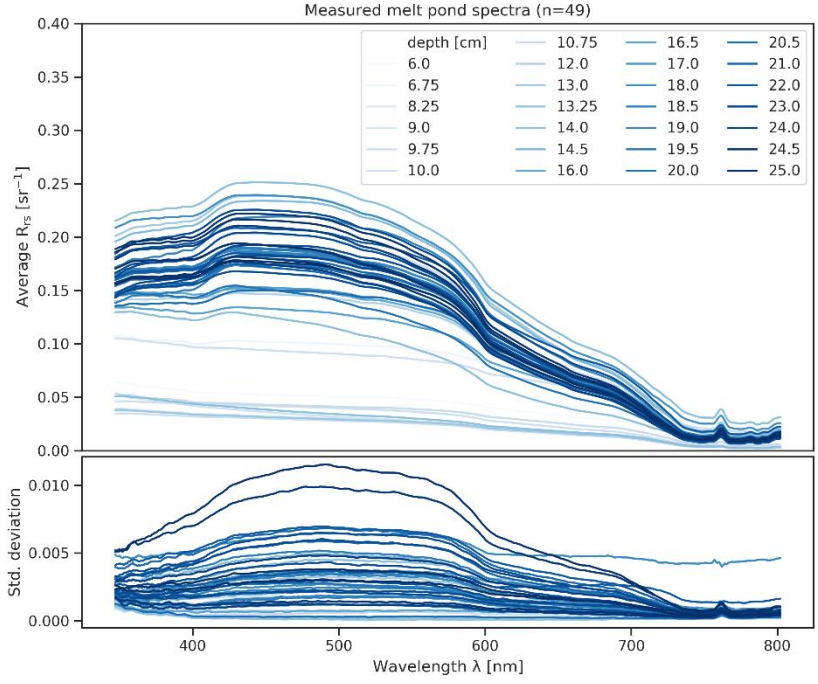

Figure 4: Average reflectance spectra (top), standard deviations of 30 measurements (bottom) and corresponding pond depths.

2.1.3 Data smoothing

Even though the spectra appear smooth at first view, the hardly visible amount of noise in the data becomes relevant for calculating derivatives. To smooth the spectra, we therefore resampled all spectra to a 1 nm spectral sampling by linear interpolation, and then applied a running average filter with a width of 5 nm.

2.2 Model development

To develop an approach that does not require expert knowledge, our model must be independent from changes of the bottom albedo, i.e. scattering characteristics of the underlying ice. It shall further be applicable to a wide range of pond depths up to 1.0 m. Because the in situ melt pond dataset is limited to shallow depths and biased towards bright blueish ponds, we used the Water Color Simulator (WASI) to create a spectral library covering different bottom type mixtures and depths. WASI is a

https://doi.org/10.5194/tc-2019-261
Preprint. Discussion started: 9 December 2019

100 software tool for the analysis and simulation of deep- and shallow-water spectra that bases on well-established analytical models (Gege, 2004, 2014, 2015; Gege and Albert, 2006). We used the forward mode of the program WASI-2D (v4.1) to generate spectral libraries of melt pond spectra. The procedures are described in the following.

2.2.1 Simulated data

We used the Ocean Optics bare ice spectra from overcast sky conditions (Sect. 2.1.1 Ice spectra) as pond bottom reflectance.
105 Analyses of optical properties of water samples showed only negligible amounts of chlorophyll-a, colored dissolved organic matter and total suspended matter. Moreover, Podgorny and Grenfell (1996) report that the signal of scattering in melt water is overwhelmed by the scattering in the bottom ice. We therefore defined a pure water column without absorbing or scattering water constituents and computed remote sensing reflectance in shallow water above the water surface according to Eq. 2.20b in Gege (2015):

110 $$R_{rs}^{sh}(\lambda) = \frac{(1-\sigma)(1-\sigma_L^-)}{n_w^2} \cdot \frac{R_{rs}^{sh-}(\lambda)}{1-\rho_u \cdot Q \cdot R_{rs}^{sh-}(\lambda)} + R_{rs}^{surf}(\lambda)\,, \quad (4)$$

where σ, σ_L^- and ρ_u are the reflection factors for E_d and upwelling radiance (L_u^-) and irradiance just below the water surface. σ and ρ_u are 0.03 and 0.54, respectively, while σ_L^- is calculated from the viewing angle (0° for a nadir-directed sensor). n_w is the refractive index of water (≈ 1.33) and Q is a measure of the anisotropy of the light field in water, approximated as 5 sr. R_{rs}^{sh-} is the remote sensing reflectance just below the water surface according to Albert and Mobley (2003):

115 $$R_{rs}^{sh-}(\lambda) = R_{rs}^{-}(\lambda) \cdot \left[1 - A_{rs,1} \cdot \exp\left\{-\left(K_d(\lambda) + k_{uW}(\lambda)\right) \cdot z_B\right\}\right] + A_{rs,2} \cdot R_{rs}^{b}(\lambda) \cdot \exp\{-K_d(\lambda) + k_{uB}(\lambda)) \cdot z_B\}, \quad (5)$$

where $A_{rs,1}$ and $A_{rs,2}$ are empirical constants, K_d, k_{uW} and k_{uB} describe the attenuation of the water body with depth z_B defined by its absorption and backscattering, and the viewing and illumination geometry. The first part of Eq. (5) describes the contribution of the water body and the second part the contribution of the bottom. R_{rs}^{-} is the remote sensing reflectance of deep water just below the water surface defined by absorption and backscattering of the water body and the viewing and illumination
120 geometry. R_{rs}^{b} is the remote sensing reflectance of the bottom that is defined as the sum of the fractional radiances of all contributing bottom types defined by their albedos and under the assumption of isotropic reflection. R_{rs}^{surf} in Eq. (4) is the ratio of radiance reflected by the water surface and E_d. We set R_{rs}^{surf} to zero; thus, the last part of Eq. (4) can be ignored. We further used a sun zenith angle of 60°, similar to the in situ measurements, and a viewing angle of 0° (nadir).
We computed linear mixtures of the two measured bottom albedos in 25 % steps (100 % dark, 0 % bright; 75 % dark, 25 %
125 bright; …; 0 % dark, 100 % bright). Using this setup, we generated a spectral look up table (LUT) by increasing pond depth from 0 to 100 cm in intervals of 1 cm. The final LUT contains 505 spectra (Figure 5).

https://doi.org/10.5194/tc-2019-261
Preprint. Discussion started: 9 December 2019

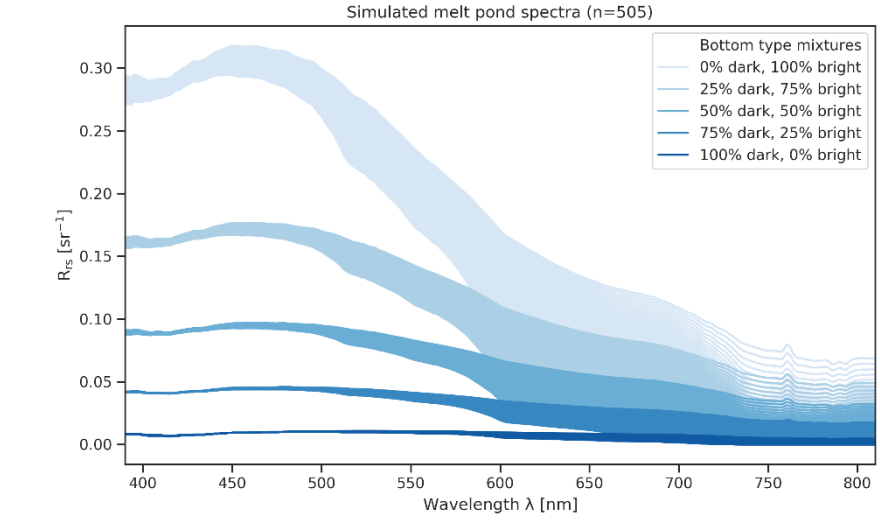

Figure 5: LUT generated with WASI-2D. Each of the five bottom type mixtures consists of 101 spectra (0 cm to 100 cm in 1 cm steps).

2.2.2 Data Processing

According to the Beer–Lambert law, the extinction of light at a certain wavelength in a medium is described by an exponential function. Figure 6A illustrates the exponential decrease of R_{rs} with water depth at 700 nm for the five different bottom type mixtures. To linearize the effect, we computed the logarithm of the spectra (Figure 6B). Lastly, we computed the first derivative of the logarithmized spectra (Figure 6C) for each band by applying a Savitzky-Golay filter using a second order polynomial fit on a 9 nm window (The Scipy community, 2019b).

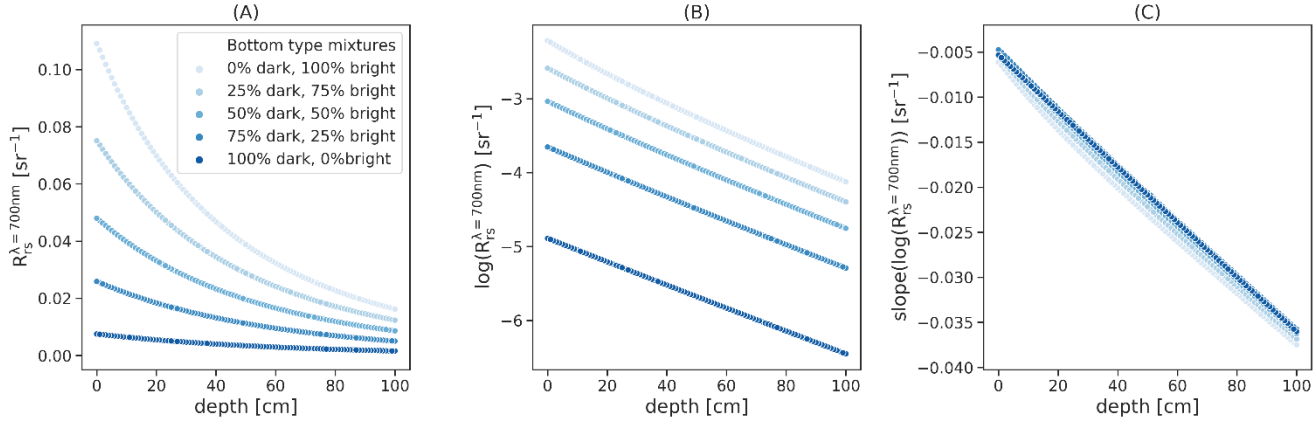

Figure 6: Processing of spectral data exemplified for λ = 700 nm.

We then computed Pearson's correlation coefficient (r) as (The Scipy community, 2019c):

https://doi.org/10.5194/tc-2019-261
Preprint. Discussion started: 9 December 2019

$$r(x,y) = \frac{\sum_{i=0}^{n-1}(x_i - \acute{x})(y_i - \acute{y})}{\sqrt{\sum_{i=0}^{n-1}(x_i - \acute{x})^2 \sum_{i=0}^{n-1}(y_i - \acute{y})^2}}, \quad (6)$$

where x_i and $\acute{x}$ are the depth of the i-th sample and the average depth and y_i and $\acute{y}$ are the slope of the logarithmized reflectance at a certain wavelength of the i-th sample and the average slope of the logarithmized reflectance at a certain wavelength; and n is the number of samples.

The orange curve in Figure 7 illustrates the wavelength dependent correlation coefficients of the slope of the logarithmized spectra and pond depths in the LUT. We observe an almost perfect negative correlation in bands between 700 nm and 750 nm. We performed the same processing as for the simulated spectra for the in situ pond spectra. The blue curve in Figure 8 illustrates the wavelength dependent correlation coefficients of measured pond depth and the slope of the logarithmized in situ spectra. We likewise observe strong negative correlations in the wavelength region around 700 nm.

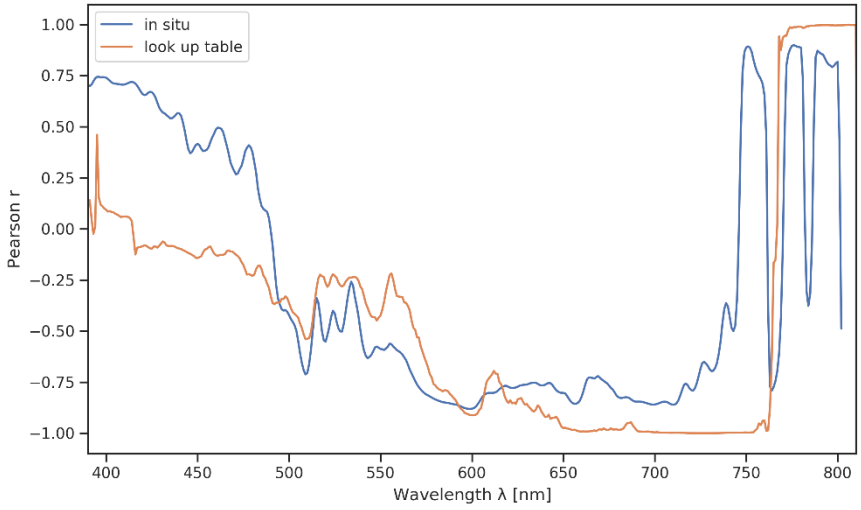

Figure 7: Wavelength dependent correlation coefficients of pond depth with slope of log-scaled spectra for in situ measurements and simulated spectra.

To investigate the similarity of the dark and bright ice spectra, we normalized both bottom spectra at 710 nm and found a high spectral similarity between ~ 590 nm and ~ 800 nm (Figure 8). Consequently, the slope of the logarithmized spectra is widely independent from the chosen bottom albedo in this wavelength region. Assuming that this also applies to ice spectra recorded under clear sky conditions, we used the Ibsen bare ice measurement to develop a model for clear sky conditions accordingly.

https://doi.org/10.5194/tc-2019-261
Preprint. Discussion started: 9 December 2019

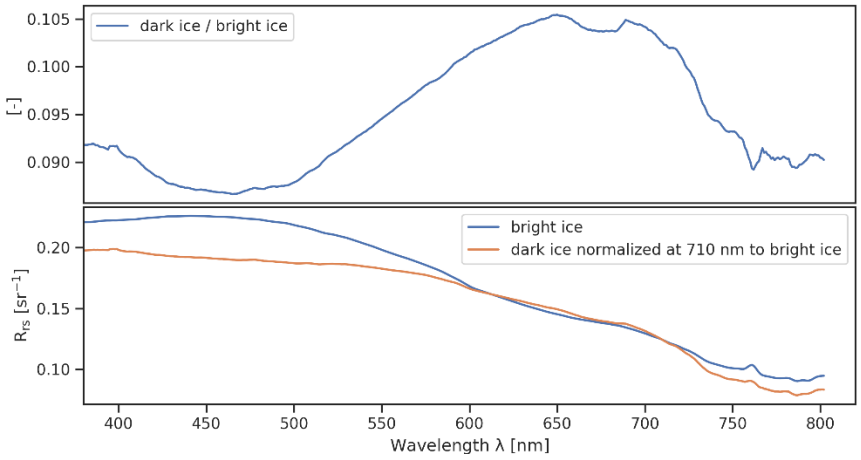

Figure 8: Quotient of bright and dark bare ice spectra (top) and R_{rs} of bright ice and dark ice normalized at 710 nm (bottom).

2.2.3 Linear model

Due to the strong negative correlation in the simulated as well as in the measured data, we chose the slope of the logarithmized spectrum at 710 nm (r = -1.0 and -0.86 for simulated and in situ data, respectively) to develop a simple linear model. We used scikit-learn's Linear Regression function (Pedregosa et al., 2011) to fit a linear model to the simulated data with the Ibsen bare ice spectrum as bottom albedo using the method of Ordinary Least Squares.

We found that the solar zenith angle affects the slope and y-intercept of the linear model. Because the model shall be applicable to a wide range of sun zenith angles, we implemented a second model to derive slope and y-intercept of the linear model for various sun zenith angles. We used WASI to generate spectral libraries for different sun zenith angles (0°, 15°, 30°, 45°, 60°, 75°, 90°) and found that the resulting change of slope and y-intercept can each be described by an s-shaped curve. We used SciPy's optimize.curve_fit function (The Scipy community, 2019a) to fit generalized logistic functions (Richards, 1959) into the data. Using these functions, the model's slope and y-intercept can be computed for different sun zenith angles (Figure 9).

https://doi.org/10.5194/tc-2019-261
Preprint. Discussion started: 9 December 2019

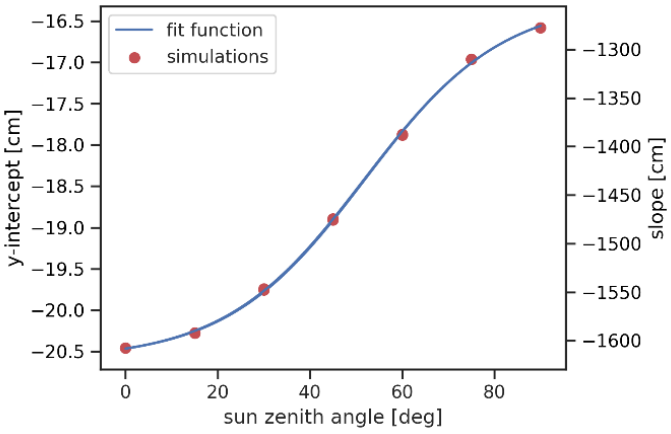

Figure 9: Change of model's y-intercept and slope with sun zenith angle. Generalized logistic function fit into the simulated data.

The model is

$$z = a(\theta_{sun}) + b(\theta_{sun}) \left[\frac{\partial log\ R_{rs}(\lambda)}{\partial \lambda}\right]_{\lambda=710\ nm} \quad (7)$$

where z is the predicted pond depth and θ_{sun} is the sun zenith angle. a and b are offset and slope:

$$a(\theta_{sun}) = -20.6 + \frac{0.79}{0.8+5.8\exp(-0.13\cdot\theta_{sun})^{\frac{1}{2}}}\ [cm] \quad (8)$$

and

$$b(\theta_{sun}) = -1619.8 + \frac{94743.64}{255.3+7855\exp(-1.3\cdot\theta_{sun})^{\frac{1}{19.9}}}\ [cm] \quad (9)$$

We further computed the coefficient of determination (R^2) as recommended by Kvålseth (1985) as:

$$R^2(y,\hat{y}) = 1 - \frac{\sum_{i=0}^{n-1}(y_i-\hat{y}_i)^2}{\sum_{i=0}^{n-1}(y_i-\acute{y})^2}, \quad (10)$$

where y_i and $\hat{y}_i$ are the true (simulated) and predicted value of the i-th sample, n is the number of samples and $\acute{y}_i = \frac{1}{n}\sum_{i=0}^{n-1} y_i$ (Pedregosa et al., 2011; scikit-learn developers, 2018b). In addition, we also computed the root-mean-square error ($RMSE$) according to Pedregosa et al. (2011) and scikit-learn developers (2018a) as:

$$RMSE(y,\hat{y}) = \sqrt{\frac{1}{n}\sum_{i=0}^{n-1}(y_i-\hat{y}_i)^2}, \quad (11)$$

https://doi.org/10.5194/tc-2019-261
Preprint. Discussion started: 9 December 2019

For the model described above we obtained a perfect correlation (r = 1.0; probability value (p) = 8.9e^{-172}), an R^2 of 1.0 and an $RMSE$ of 0.56 cm on the simulated training data.

3 Results

We validated the model with the in situ melt dataset from dark and bright ponds (Sect. 2.1.2 Pond) and observed a strong linear and statistically significant correlation (r = 0.86; p = 2.36e^{-15}; R^2 = 0.65 and $RMSE$ = 3.29 cm). Most of the points scatter along the 1:1 line, except for one point where actual depth is 10 cm and predicted depth is 18.17 cm (Figure 10A). The externally studentized residual (t) (Kutner et al., 2004; Seabold and Perktold, 2010) classifies this point as an outlier (t > 3) and therefore we excluded this point from the data set. The removal of the outlier improves all performance measures (r = 0.89; p = 4.34e^{-17}, R^2 = 0.68, $RMSE$ = 3.11 cm). The slope of the line of best-fit increases to 0.9686 and the intercept indicates an offset of 0.878 cm. If we further correct for the offset R^2 increases to 0.74 and $RMSE$ improves to 2.81 cm The blue line is the line of best fit between actual and predicted pond depths. The linear equation of the line of best fit indicates that the model results in a small offset and a slope close to 1.0.

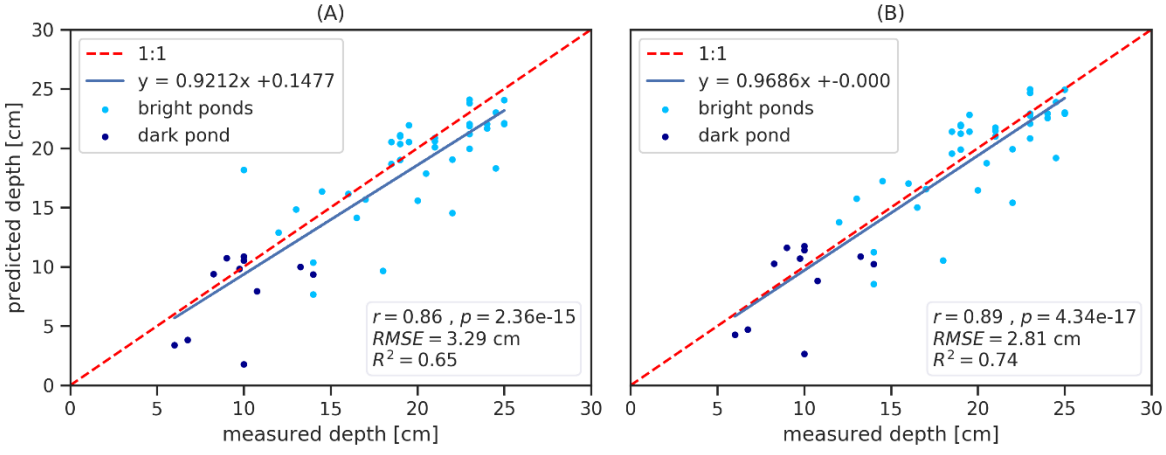

Figure 10: Measured vs. predicted depth for the entire dataset (A), with outlier removed and offset correction (B).

4 Discussion

Our results show that a simple model based on the derivative of the log-scaled R_{rs} at 710 nm allows water depth retrieval of dark and bright melt ponds on Arctic sea ice. The model training on simulated data and the independent testing using in situ measurements prove the universality of our approach.

https://doi.org/10.5194/tc-2019-261
Preprint. Discussion started: 9 December 2019

4.1 Observational data

To our knowledge, the data used in this study is the most comprehensive set of R_{rs} and depth measurements from Arctic melt ponds acquired under clear sky conditions.

4.1.1 Spectral measurements

Measurement of albedo have a long tradition in Arctic research (e.g. Grenfell, 2004; Nicolaus et al., 2010; Perovich, 2002; Perovich and Polashenski, 2012) because albedo is an important quantity in climate models and can be measured with a single irradiance detector. In this study, we conducted measurements of R_{rs} because it is the most popular quantity in remote sensing and less sensitive to external environmental conditions while being sensitive to the inherent optical properties of a water body (Mobley et al., 2018). Morassutti and Ledrew (1996) identified changing E_d as the main error affecting reflectance data recording. To tackle this issue, we used a combination of two spectrometers described in Sect. 2.1 Observational data.

Field spectroscopy is influenced by external factors and the measurement design itself. In contrast to ruler measurements, the spectrometer acquires information of an area. To ease comparison and limit the influence of spatial heterogeneities, we used a fore optic with a 1° FOV to minimize the footprint (~ 1 cm at a height of 60 cm). However, holding the instruments perfectly still for a period of several seconds is challenging and even small changes in the position result in changes of the viewing angle, which increase the footprint of a measurement. For future campaigns, we therefore recommend using a gimbal to minimize the influence of roll and pitch of the hand-held spectrometer setup. Another issue might have been reflections of the black spectrometer housings at the water surface possibly contribute to the offset between modeled and measured data. Different refraction indices of wet and dry surfaces may cause part of the observed offset. Furthermore, using bottom albedos obtained from dry surfaces in WASI introduce a systematic offset. However, it remains unclear if the ice surface used to compute the spectral library was wet or dry.

Some of the scattering may be introduced by reflectances at the water surface, which we did not consider in the LUT computation because the necessary values for the parametrization are unknown. Another influence may be the different sun zenith angle between bare ice and pond measurements. The potential influence of the mentioned factors may be worth further examination to refine the model.

4.1.2 Pond depth measurements

Measuring the depth of a pond may appear trivial but the bottom of a pond is frequently not flat and solid but can be slushy or riddled with holes. In addition, hitting the exact same spot of the spectral measurement perpendicularly with a folding ruler is tricky. We therefore recommend using a laser pointer at the end of the pole for orientation. These uncertainties explain some of the scattering in Figure 10. Interpretation of field photographs of the pond bottoms however did not indicate any systematic errors associated with pond bottom characteristics.

https://doi.org/10.5194/tc-2019-261
Preprint. Discussion started: 9 December 2019

4.2 Model validity

The majority of the field data used in this study is from bright blue ponds (n=38) while fewer measurements were obtained in dark ponds (n=11). We addressed this limited diversity of field data by computing a comprehensive LUT. The model generates accurate results ($RMSE$ = 2.81 cm) on the in situ test data set and explains a large portion of its variability (R^2 = 0.74), but further investigation is necessary to explore its capabilities to derive pond depths > 25 cm. In addition, more tests are necessary to explore how the model performs when the assumptions formulated in Sect. 2.2 are violated, e.g. when algae, suspended matter or yellow substances are abundant in the pond water or in the ice below the pond.

We successfully developed a model that is widely independent from the bottom ice characteristics of the pond; yet, we assume that we cannot entirely avoid any influence. When fitting a model to the Ocean Optics LUT (Figure 6C), we observe scattering around the 1:1 line resulting in $RMSE$ of 1.88 cm. In the Ocean Optics LUT, however, the only variable parameter is bottom type mixture; we therefore conclude that the scattering results from the difference in bottom albedo. Consequently, bottom albedo may affect the model, which may explain some of the scattering in the test data.

Optical satellite data can only be obtained under clear sky conditions but remote sensing images are likewise acquired from helicopters and UAVs. These platforms also operate under diffuse illumination conditions, which are frequent in the Arctic. To check the validity of the model for overcast conditions, we applied the clear sky model to data from the same area acquired on 14 June 2017 during diffuse illumination conditions. The performance, however, is low (Figure 11) and shows a moderate correlation (r = 0.64; p = 2.6e^{-4}), an $R^2 < 0$ and an $RMSE$ of 12.76 cm. We attribute the low performance to the different illumination conditions. Under diffuse conditions a considerable part of the reflectance measured above the water surface is due to reflection of clouds at the water surface. Further, the optical path length of the incoming light in water changes under overcast conditions.

We therefore conclude that due to the settings of the field measurements, the present model is valid for clear sky conditions with sun zenith angles between 58.9° and 61°. To enlarge its validity range more field data covering different weather and illumination conditions is necessary.

https://doi.org/10.5194/tc-2019-261
Preprint. Discussion started: 9 December 2019

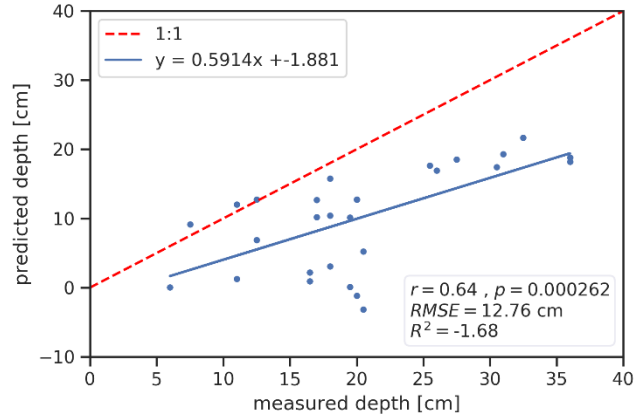

Figure 11: Measured vs. predicted water depth for data acquired under overcast conditions on 14 June 2017.

5 Conclusion

We present a model based on a slope approach in the spectral region around 710 nm to retrieve the depth of melt ponds on Arctic sea ice. The separation of model calibration on simulated data and validation on in situ data proves the universality of our approach. The final model is valid for hyperspectral data (R_{rs}) acquired under clear sky conditions and has been tested on a range of sun zenith angles between 58.9° and 61°.

We used WASI to generate a LUT of pond spectra for five different bottom albedos and pond depths between 0 and 100 cm assuming clear pond water. We found that the slope of the log-scaled R_{rs} at 710 nm is widely independent from the bottom albedo and highly correlated with pond depth. Thus, we applied a linear model to retrieve pond depth from R_{rs} in this wavelength region. Slope and y-intercept of the linear equation, however, change with sun zenith angle. To overcome this limitation, we trained linear models for seven sun zenith angles and found that a general logistic function is able to describe the change of slope and y-intercept for each sun zenith angle. The inputs for our model therefore are the slope of the log-scaled $R_{rs}^{\lambda=710}$ and sun zenith angle. We successfully validated the model on in situ measurements from bright and dark ponds (R^2 = 0.74, $RMSE$ = 2.81 cm).

The next step is the transfer to hyperspectral airborne and satellite systems, e.g. EnMAP (Guanter et al., 2016), to enable a synoptic view on the evolution of melt ponds in Arctic sea ice. One constraint may be the size of melt ponds, especially during melt onset and early pond development, which requires a high spatial resolution. We further assume that the additive signals of the water surface and the atmosphere on the spectrum measured at a satellite sensor may complicate the retrieval of pond depth. In addition, the sensitivities and band settings of remote sensors also affect the transferability of our approach. Here, further testing and comprehensive ground truth data is necessary. In these regards, we expect the Multidisciplinary drifting Observatory for the Study of Arctic Climate (MOSAiC) expedition to result in further improvements.

https://doi.org/10.5194/tc-2019-261
Preprint. Discussion started: 9 December 2019

References

Albert, A. and Mobley, C.: An analytical model for subsurface irradiance and remote sensing reflectance in deep and shallow case-2 waters, Opt. Express, 11(22), 2873, doi:10.1364/OE.11.002873, 2003.

Curry, J. a., Schramm, J. L. and Ebert, E. E.: Sea Ice-Albedo Climate Feedback Mechanism, J. Clim., 8(2), 240–247, doi:10.1175/1520-0442(1995)008<0240:SIACFM>2.0.CO;2, 1995.

Gege, P.: The water color simulator WASI: an integrating software tool for analysis and simulation of optical in situ spectra, Comput. Geosci., 30(5), 523–532, doi:10.1016/j.cageo.2004.03.005, 2004.

Gege, P.: WASI-2D: A software tool for regionally optimized analysis of imaging spectrometer data from deep and shallow waters, Comput. Geosci., 62, 208–215, doi:10.1016/j.cageo.2013.07.022, 2014.

Gege, P.: The Water Colour Simulator WASI User manual for WASI version 4.1., 2015.

Gege, P. and Albert, A.: A Tool for Inverse Modeling of Spectral Measurements in Deep and Shallow Waters, Situ, 81–109, 2006.

Gege, P. and König, M.: HCRF measurements (Ibsen Freedom VIS FSV-305) of bare Arctic sea ice acquired during POLARSTERN cruise PS106/2, , doi:doi.pangaea.de/10.1594/PANGAEA.908073, 2019.

Gege, P., König, M. and Oppelt, N.: Reflectance measurements (Ocean Optics STS-VIS) of bare ice and melt ponds on Arctic sea ice acquired during POLARSTERN cruise PS106/1, , doi:doi.pangaea.de/10.1594/PANGAEA.908074, 2019.

Grenfell, T. C.: Seasonal and spatial evolution of albedo in a snow-ice-land-ocean environment, J. Geophys. Res., 109(C1), C01001, doi:10.1029/2003JC001866, 2004.

Guanter, L., Kaufmann, H., Foerster, S., Brosinsky, A., Wulf, H., Bochow, M., Boesche, N., Brell, M., Buddenbaum, H., Chabrillat, S., Hank, T., Heiden, U., Heim, B., Heldens, W., Hill, J., Hollstein, A., Hostert, P., Krasemann, H., Leitão, P. J., van der Linden, S., Mauser, W., Mielke, C., Müller, A., Oppelt, N., Roessner, S., Röttgers, R., Schneiderhan, T., Staenz, K. and Segl, K.: EnMAP Science Plan. EnMAP Technical Report., 2016.

Ibsen Photonics: FREEDOM VIS Product Sheet, [online] Available from: https://ibsen.com/wp-content/uploads/Ibsen-Product-Sheets-FREEDOM-VIS.pdf, 2019.

Kutner, M. H., Li, W., Nachtsheim, C. J. and Neter, J.: Applied Linear Statistical Models, Fifth edit., 2004.

Kvålseth, T. O.: Cautionary Note about R 2, Am. Stat., 39(4), 279–285, doi:10.1080/00031305.1985.10479448, 1985.

Lu, P., Leppäranta, M., Cheng, B. and Li, Z.: Influence of melt-pond depth and ice thickness on Arctic sea-ice albedo and light transmittance, Cold Reg. Sci. Technol., 124, 1–10, doi:10.1016/j.coldregions.2015.12.010, 2016.

Lu, P., Leppä, M., Cheng, B., Li, Z., Istomina, L. and Heygster, G.: The color of melt ponds on Arctic sea ice, , 8(August), 1–24, 2017.

Malinka, A., Zege, E., Istomina, L., Heygster, G., Spreen, G., Perovich, D. and Polashenski, C.: Reflective properties of melt ponds on sea ice, Cryosph., 12(6), 1921–1937, doi:10.5194/tc-12-1921-2018, 2018.

Mobley, C. D., Boss, E. and Roesler, C.: Ocean Optics Web Book, [online] Available from: http://www.oceanopticsbook.info/

(Accessed 17 May 2018), 2018.

Morassutti, M. P. and Ledrew, E. F.: Albedo and depth of melt ponds on sea-ice, Int. J. Climatol., 16(7), 817–838, 1996.

Nicolaus, M., Gerland, S., Hudson, S. R., Hanson, S., Haapala, J. and Perovich, D. K.: Seasonality of spectral albedo and transmittance as observed in the Arctic Transpolar Drift in 2007, J. Geophys. Res. Ocean., 115(11), 1–21, doi:10.1029/2009JC006074, 2010.

Ocean Optics: STS-VIS SPECS, [online] Available from: https://oceanoptics.com/product/sts-vis-microspectrometer/#tab-specifications (Accessed 26 March 2019), 2019.

Pedregosa, F., Varoquaux, G., Gramfort, A., Michel, V., Thirion, B., Grisel, O., Blondel, M., Prettenhofer, P., Weiss, R., Dubourg, V., Vanderplas, J., Passos, A., Cournapeau, D., Brucher, M., Perrot, M. and Duchesnay, E.: Scikit-learn: Machine Learning in {P}ython, J. Mach. Learn. Res., 12, 2825–2830, 2011.

Perovich, D. K.: Seasonal evolution of the albedo of multiyear Arctic sea ice, J. Geophys. Res., 107(C10), 1–13, doi:10.1029/2000JC000438, 2002.

Perovich, D. K. and Polashenski, C.: Albedo evolution of seasonal Arctic sea ice, Geophys. Res. Lett., 39(8), 1–6, doi:10.1029/2012GL051432, 2012.

Podgorny, I. A. and Grenfell, T. C.: Partitioning of solar energy in melt ponds from measurements of pond albedo and depth, J. Geophys. Res. Ocean., 101(C10), 22737–22748, doi:10.1029/96JC02123, 1996.

Pope, R. M. and Fry, E. S.: Absorption spectrum (380–700 nm) of pure water II Integrating cavity measurements, Appl. Opt., 36(33), 8710, doi:10.1364/AO.36.008710, 1997.

Richards, F. J.: A Flexible Growth Function for Empirical Use, J. Exp. Bot., 10(2), 290–301, doi:10.1093/jxb/10.2.290, 1959.

Schröder, D., Feltham, D. L., Flocco, D. and Tsamados, M.: September Arctic sea-ice minimum predicted by spring melt-pond fraction, Nat. Clim. Chang., 4(5), 353–357, doi:10.1038/nclimate2203, 2014.

scikit-learn developers: Mean squared error, [online] Available from: https://scikit-learn.org/stable/modules/model_evaluation.html#mean-squared-error (Accessed 13 February 2019a), 2018.

scikit-learn developers: R^2 score, the coefficient of determination, [online] Available from: https://scikit-learn.org/stable/modules/model_evaluation.html#r2-score (Accessed 13 February 2019b), 2018.

Seabold, S. and Perktold, J.: Statsmodels: Econometric and statistical modeling with python, in 9th Python in Science Conference., 2010.

The Scipy community: scipy.optimize.curve_fit, SciPy v1.2.1 Ref. Guid. [online] Available from: https://docs.scipy.org/doc/scipy/reference/generated/scipy.optimize.curve_fit.html (Accessed 11 July 2019a), 2019.

The Scipy community: scipy.signal.savgol_filter, SciPy v1.2.1 Ref. Guid. [online] Available from: https://docs.scipy.org/doc/scipy/reference/generated/scipy.signal.savgol_filter.html?highlight=savgol#scipy.signal.savgol_filter, 2019b.

The Scipy community: scipy.stats.pearsonr, SciPy v1.2.1 Ref. Guid. [online] Available from: https://docs.scipy.org/doc/scipy/reference/generated/scipy.stats.pearsonr.html (Accessed 13 February 2019c), 2019.

https://doi.org/10.5194/tc-2019-261
Preprint. Discussion started: 9 December 2019

350

Data availability

The data used in this study are available at the PANGAEA data repository under doi.pangaea.de/10.1594/PANGAEA.908075.

Author contribution

MK and NO conceptualized the study. MK designed the methodology, curated and analysed the data, created and validated
355 the models, visualized results and wrote the original draft. NO critically reviewed the draft and both authors contributed in editing and finalizing the paper.

Competing interests

The authors declare that they have no conflict of interest.

Acknowledgements

360 We thank Peter Gege for his encouragement and the provision of WASI. We highly appreciate the support by the German Aerospace Center (DLR) Oberpfaffenhofen and especially thank Thomas Schwarzmaier, Stefan Plattner and Peter Gege for the development and provision of the instruments used in this study. We further acknowledge the support of captain Wunderlich, the crew and the chief scientists Andreas Macke and Hauke Flores of RV Polarstern cruise AWI_PS106_00 and value the assistance provided by the colleagues supporting our fieldwork on PS106 especially Peter Gege, Gerit Birnbaum,
365 Niels Fuchs, Martin Hieronymi and Thomas Ruhtz. We would also like to thank Justin Mullins at Write About Science for his valuable comments.